

# Helical $f$ -Wave Superconductivity in Cubic Rashba Superconductors

Qi-Sheng Xu,<sup>1,\*</sup> Zi-Ming Wang,<sup>1,\*</sup> Lun-Hui Hu,<sup>2,†</sup> Rui Wang,<sup>1,3,‡</sup> and Dong-Hui Xu<sup>1,3,§</sup>

<sup>1</sup>Department of Physics and Chongqing Key Laboratory for Strongly Coupled Physics, Chongqing University, Chongqing 400044, China

<sup>2</sup>Center for Correlated Matter and School of Physics, Zhejiang University, Hangzhou 310058, China

<sup>3</sup>Center of Quantum Materials and Devices, Chongqing University, Chongqing 400044, China

(Dated: August 6, 2024)

Linear-in- $k$  Rashba spin-orbit coupling is crucial for achieving topological superconductivity. The wave vector dependence of this spin-orbit coupling can vary across materials, exhibiting linear, cubic, or a combination of both forms. Notably, cubic Rashba spin-orbit coupling induces a distinct triple spin winding on the Fermi surface, differentiating it from linear Rashba spin-orbit coupling. In this Letter, we investigate the potential for two-dimensional topological superconductivity in an interacting bilayer Rashba spin-orbit coupled system with local inversion symmetry breaking. We discover an intriguing interplay between the unique spin texture induced by cubic Rashba spin-orbit coupling and odd-parity Cooper pairing mechanisms. This interplay leads to a mirror symmetry-protected topological crystalline superconductor hosting three pairs of Majorana edge modes associated with an effective helical  $f$ -wave Cooper pairing. The bulk topology of the helical  $f$ -wave superconductor is characterized by a mirror Chern number  $n_M = 3$ , which remains stable even in the presence of coexisting linear and cubic Rashba spin-orbit couplings. Our work not only proposes an approach to engineering topological mirror superconductors but also uncovers a pathway to realizing rare helical  $f$ -wave pairing.

**Introduction.**—Spin-orbit coupling (SOC) is a relativistic effect in solids that arises from the Dirac equation, coupling the electron’s spin to its orbital degrees of freedom. In crystals lacking inversion symmetry, a specific SOC called Rashba SOC emerges, giving rise to a momentum-dependent spin splitting of energy bands [1]. Rashba SOC unlocks a treasure trove of fundamentally new phenomena [2, 3]. Examples include the spin Hall effect, where a flowing charge current can generate a transverse spin current [4]. It also plays a crucial role in shaping the helical spin texture observed on the surface of topological insulators [5, 6], can even induce mixing between spin singlet and triplet superconductivity [7] and enhance the critical field of superconductivity [7–9]. Surprisingly, Rashba SOC can even appear in centrosymmetric materials with local inversion symmetry breaking [10–12], such as bismuth-based cuprate [11] and heavy fermion superconductors [12]. This discovery has sparked an intensive study of unconventional superconductivity in locally noncentrosymmetric crystals [13], particularly odd-parity Cooper pairings.

Rashba SOC is a cornerstone for realizing topological superconductors, a unique state of matter harboring exotic Majorana quasiparticles. Various strategies involving linear Rashba-type SOC have been proposed to generate topological superconductivity through topologically trivial superconductors. A prominent example is the Fu-Kane proposal [14], where an  $s$ -wave superconductor in proximity to a topological insulator with a helical spin-textured surface induces effective  $p$ -wave pairing, supporting zero-energy Majorana bound states at the core of superconducting vortices. Further studies have revealed that by breaking time-reversal symmetry and mirror symmetries, two-dimensional (2D) topologically chiral  $p$ -wave superconductivity, characterized by a non-zero Chern number, can be realized in more conventional systems by combining Rashba SOC with an applied magnetic field [15–18]. Additionally, there are proposals to realize 2D helical topological superconductors, classified by a  $\mathbb{Z}_2$  topological invariant,

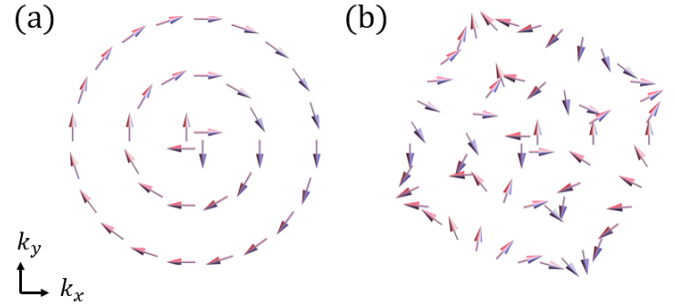


FIG. 1. (a) and (b) represent schematic illustrations of the spin texture of the splitted Fermi surfaces by the linear Rashba SOC and cubic Rashba SOC, respectively.

using Rashba spin-orbit coupled systems with or without inversion symmetry [19–21].

Recently, a higher-order Rashba SOC, which is cubic in wave vector as required by the time-reversal symmetry, has garnered significant attention and plays important roles in several materials [22–28]. Unlike the spin-momentum locking caused by linear Rashba, cubic Rashba exhibits a “triple winding” effect, where electron spins make three complete rotations within the plane as their momentum changes [see Fig. 1]. This leads to intriguing phenomena like large spin Hall conductivity and unique spin-spin correlations [23, 29–31]. More interestingly, time-reversal-symmetry breaking proximity-induced  $f$ -wave superconductivity in one or two dimensions can be achieved by combining cubic Rashba SOC with conventional  $s$ -wave pairing under a magnetic field [32–34]. However, while these initial studies have illuminated the interplay between cubic Rashba SOC and superconductivity, the time-reversal invariant superconductivity in such systems remains unexplored.

In this Letter, we investigate time-reversal invariant helical topological superconductivity in a cubic Rashba spin-orbit

coupled superconductor with local inversion symmetry breaking. We employ an interacting bilayer cubic Rashba spin-orbit coupled model and perform mean-field calculations to unveil the superconducting phase diagram. Our findings reveal that when the chemical potential resides within the hybridization gap opened by the interlayer coupling, odd-parity Cooper pairings give rise to an intriguing topological crystalline superconductor protected by the out-of-plane mirror symmetry. This state harbors three pairs of helical Majorana edge modes. Further analysis indicates that an effective helical  $f$ -wave pairing is realized, with the bulk topology characterized by a mirror Chern number  $n_M = 3$ . The topological helical  $f$ -wave superconductor persists in systems exhibiting both linear and cubic Rashba SOC.

**Model.**—For our purpose, we consider a simple low-energy continuous model describing the normal state of a bilayer structure based on the  $D_{4h}$  space group, where the Rashba SOC arises from the local inversion symmetry breaking. The Hamiltonian reads

$$\mathcal{H}_n(\mathbf{k}) = \epsilon_0(\mathbf{k})\tau_0 \otimes s_0 + \tau_z \otimes [\mathbf{g}(\mathbf{k}) \cdot \mathbf{s}] + \varepsilon\tau_x \otimes s_0, \quad (1)$$

where  $\epsilon_0(\mathbf{k}) = \beta_0 k^4 + \beta_1 k^2$  denotes the kinetic energy,  $\mathbf{g}(\mathbf{k}) = \alpha_{\text{LR}}(-k_y, k_x, 0) + \alpha_{\text{CR}}[-k_y(3k_x^2 - k_y^2), k_x(3k_y^2 - k_x^2), 0]$  describes the Rashba SOC including both linear order ( $\alpha_{\text{LR}}$ ) and cubic order ( $\alpha_{\text{CR}}$ ) terms.  $\varepsilon$  represents the coupling of two layers, as shown in Fig. 2(a), which leads to a hybridization gap around the  $\Gamma$  point as shown in Fig. 2(b).  $\tau_{x,y,z}$  and  $s_{x,y,z}$  represent the Pauli matrices of layer and spin degrees of freedom, respectively,  $\tau_0$  and  $s_0$  are the  $2 \times 2$  identity matrix. For simplicity, we consider short-range electron density-density interaction [20, 35, 36] for superconductivity

$$H_{\text{int}}(\mathbf{r}) = -U[n_L^2(\mathbf{r}) + n_U^2(\mathbf{r})] - 2Vn_L(\mathbf{r})n_U(\mathbf{r}), \quad (2)$$

where  $n_{\tau=L,U}(\mathbf{r}) = \sum_{s=\uparrow,\downarrow} c_{\tau,s}^\dagger(\mathbf{r})c_{\tau,s}(\mathbf{r})$  denotes the particle number of the upper and lower layers.  $U$  and  $V$  represent the strength of intra-layer and inter-layer interactions, respectively. We then solve  $H_n + H_{\text{int}}$  using the standard mean-field approximation, which involves decomposing Eq. (2) into orbital-dependent but  $\mathbf{k}$ -independent pairing potential. By introducing the Nambu spinor  $\psi_{\mathbf{k}}^\dagger = (c_{L\mathbf{k},\uparrow}^\dagger, c_{L\mathbf{k},\downarrow}^\dagger, c_{U\mathbf{k},\uparrow}^\dagger, c_{U\mathbf{k},\downarrow}^\dagger, c_{L-\mathbf{k},\uparrow}, c_{L-\mathbf{k},\downarrow}, c_{U-\mathbf{k},\uparrow}, c_{U-\mathbf{k},\downarrow})$ , the Bogoliubov-de Gennes (BdG) Hamiltonian is given by

$$\mathcal{H}_{\text{BdG}}(\mathbf{k}) = \begin{pmatrix} \mathcal{H}_n(\mathbf{k}) - \mu & \Delta(\mathbf{k}) \\ \Delta^\dagger(\mathbf{k}) & -\mathcal{H}_n^*(-\mathbf{k}) + \mu \end{pmatrix}, \quad (3)$$

where  $\mu$  is the chemical potential and  $\Delta(\mathbf{k})$  is the pairing potential. We list four possible pairing potentials in Table I according to the representation of  $D_{4h}$ .  $\Delta_1$  has both intralayer pairing  $\Delta_{1a} = \Delta_0(c_{L,\uparrow}c_{L,\downarrow} + c_{U,\uparrow}c_{U,\downarrow})$  and interlayer pairing  $\Delta_{1b} = \Delta_0(c_{L,\uparrow}c_{U,\downarrow} - c_{L,\downarrow}c_{U,\uparrow})$  components, being parity even. Here,  $\Delta_0$  is the strength of pairing potential.  $\Delta_2$  and  $\Delta_3$  represent odd-parity superconducting pairings arising from interlayer and intralayer interactions, respectively.  $\Delta_{4x} = i\Delta_0(c_{L,\uparrow}c_{U,\uparrow} + c_{L,\downarrow}c_{U,\downarrow})$  and  $\Delta_{4y} = \Delta_0(c_{L,\uparrow}c_{U,\uparrow} - c_{L,\downarrow}c_{U,\downarrow})$

are odd-parity superconducting pairings involving interlayer interaction with the same spins. To reveal the topological superconductivity induced by the cubic Rashba SOC, we initially neglect the linear Rashba SOC by setting  $\alpha_{\text{LR}} = 0$ .

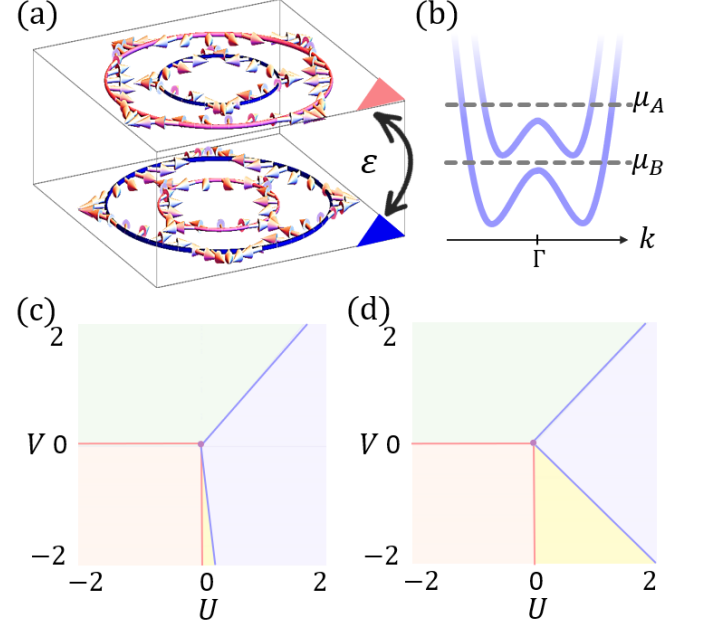


FIG. 2. (a) represents an inversion symmetric cubic Rashba bilayer, where the upper and lower layers have opposite cubic Rashba SOC, and the interlayer coupling is marked as  $\varepsilon$ . (b) The energy dispersion around the  $\Gamma$  point,  $\mu_A$  and  $\mu_B$  represent the chemical potentials outside and inside the hybridization gap induced by  $\varepsilon$ , respectively. (c) Superconducting phase diagram in case  $\mu_A$  as  $\mu = 1.5$ . (d) Superconducting phase diagram in case  $\mu_B$  as  $\mu = 0$ . The purple region denotes the  $\Delta_1$  phase, the green region indicates the  $\Delta_2$  phase, the yellow region signifies the  $\Delta_3$  phase, and the orange region is the non-superconducting phase. Common parameters,  $\beta_0 = 0.5$ ,  $\beta_1 = -1$ ,  $\varepsilon = 0.8$ ,  $\alpha_{\text{CR}} = 0.5$ .

In the weak coupling limit, we can determine superconducting critical temperature  $T_c$  by solving the linearized gap equation, which can be expressed using the pairing susceptibility. The pairing susceptibility  $\chi$  is defined as

$$\begin{aligned} \chi_{ij} &\equiv -\frac{k_B T_c}{2N} \sum_{\omega, \mathbf{k}} \text{Tr}[\gamma_i^\dagger \mathcal{G}_e(\omega, \mathbf{k}) \gamma_j \mathcal{G}_h(\omega, \mathbf{k})] \\ &= -\frac{1}{N} \sum_{\mathbf{k}} \left\{ F_{ij}^+(k) \frac{\tanh[(\xi_0 + \lambda_k - \mu)/(2k_B T_c)]}{2(\xi_0 + \lambda_k - \mu)} \right. \\ &\quad \left. + F_{ij}^-(k) \frac{\tanh[(\xi_0 - \lambda_k - \mu)/(2k_B T_c)]}{2(\xi_0 - \lambda_k - \mu)} \right\}, \end{aligned} \quad (4)$$

where  $\mathcal{G}_{e,h}$  is the normal Green's function for electrons and holes, respectively.  $k_B$  is the Boltzmann constant,  $\omega$  represents the Matsubara frequency, and  $\gamma_{i,j}$  is the matrix representations of superconducting pairing.  $\xi_0 = \beta_0 k^4 + \beta_1 k^2$ , and  $\lambda_k = \sqrt{\varepsilon^2 + \alpha_{\text{CR}}^2 k^6}$ . The coefficients  $F_{ij}^\pm$  are explicitly given in the Supplemental Materials. The linearized gap equations

TABLE I. Classification of possible pairing potentials of the short-ranged interacting model.  $\Delta_1, \Delta_2, \Delta_3$ , and  $\Delta_4$  belong to the  $A_{1g}, A_{1u}, A_{2u}$ , and  $E_u$  irreducible representations of  $D_{4h}$ , respectively. Matrix representations correspond to the off-diagonal elements of BdG Hamiltonian.

Pairing	Operator representation	Matrix	Parity
$\Delta_1$	$c_{L,\uparrow}c_{L,\downarrow} + c_{U,\uparrow}c_{U,\downarrow}, c_{L,\uparrow}c_{U,\downarrow} - c_{L,\downarrow}c_{U,\uparrow}$	$i\tau_0 s_y, i\tau_x s_y$	+
$\Delta_2$	$i(c_{L,\uparrow}c_{U,\downarrow} + c_{L,\downarrow}c_{U,\uparrow})$	$\tau_y s_x$	-
$\Delta_3$	$c_{L,\uparrow}c_{L,\downarrow} - c_{U,\uparrow}c_{U,\downarrow}$	$i\tau_z s_y$	-
$\Delta_4$	$(i(c_{L,\uparrow}c_{U,\uparrow} + c_{L,\downarrow}c_{U,\downarrow}), c_{L,\uparrow}c_{U,\uparrow} - c_{L,\downarrow}c_{U,\downarrow})$	$(\tau_y s_z, i\tau_y s_0)$	-

for different pairing channels are obtained as

$$\begin{vmatrix} U\chi_{1a} - 1 & U\chi_{1ab} \\ V\chi_{1ba} & V\chi_{1b} - 1 \end{vmatrix} = 0, \quad (5)$$

for  $\Delta_1$  channels, and

$$V\chi_2 = 1, U\chi_3 = 1, V\chi_4 = 1, \quad (6)$$

for channels  $\Delta_2, \Delta_3$  and  $\Delta_4$ . After solving these equations for each pairing channel, the superconducting phase diagram in the  $U$ - $V$  plane is determined by the maximum critical temperature  $T_c$  across all pairing channels. Figures 2(c) and 2(d) represent the phase diagram for different chemical potentials  $\mu_A$  and  $\mu_B$ , respectively.  $\mu_B$  is located within the hybridization gap, which is defined by  $(\xi_0 - \lambda_k)|_{\mathbf{k}=0} < \mu_B < (\xi_0 + \lambda_k)|_{\mathbf{k}=\mathbf{k}_0}$ , where  $\mathbf{k}_0$  represents the wave vector at which the upper band reaches its minimum value. This phase diagram showcases three distinct superconducting states  $\Delta_1, \Delta_2, \Delta_3$  competing with a non-superconducting region.  $\Delta_4$  doesn't appear in the phase diagram for the current type of electron interaction. When the intralayer attractive interaction ( $U > 0$ ) is dominant, the conventional spin-singlet pairing  $\Delta_1$  is favored, while unconventional triplet pairings  $\Delta_2$  and  $\Delta_3$  win as soon as the interlayer attractive interaction exceeds the intralayer one ( $|V| > U$ ). When both  $U$  and  $V$  are repulsive, the system is stable against superconducting instability. Notably, the region favoring  $\Delta_3$  exhibits a strong dependence on the chemical potential. This is evident when comparing the yellow regions in Figs. 2(c) and 2(d). It shrinks significantly when  $\mu$  deviates from the hybridization gap. It is necessary to point out that if superconductivity is phonon mediated, the residual electron repulsive interaction renormalizes the original values of  $U$  and  $V$ . It can be expected the strength of the repulsive interlayer interaction to be greater than the strength of intralayer attractive interaction. Therefore,  $\Delta_3$  is favored in this case.

**Topological helical  $f$ -wave superconductivity.**—In this section, we focus on the topological superconductivity induced by  $\Delta_3$ . The normal Hamiltonian preserves the following symmetries: time-reversal symmetry  $\mathcal{T} = -is_y\mathcal{K}$  with  $\mathcal{K}$  the complex conjugate, inversion symmetry  $I = \tau_x$ , and mirror symmetries  $M_y = is_y$  and  $M_z = i\tau_x s_z$ , respectively. Odd-parity  $\Delta_3$  pairing gives rise to a helical topological superconductivity protected by  $M_z$ . According to the eigenvalues  $+i$  and  $-i$  of the  $M_z$  operator, the normal Hamiltonian can be divided

into two blocks

$$\mathcal{H}_n(\mathbf{k}) = \begin{pmatrix} \mathcal{H}_{n,+i}(\mathbf{k}) & 0 \\ 0 & \mathcal{H}_{n,-i}(\mathbf{k}) \end{pmatrix}, \quad (7)$$

where  $\mathcal{H}_{n,\pm i}(\mathbf{k}) = -\epsilon_0(\mathbf{k})s_0 \pm \epsilon s_z - \mathbf{g}(\mathbf{k}) \cdot \mathbf{s}$ . Consequently, the BdG Hamiltonian has the following form

$$\mathcal{H}_{\pm i}(\mathbf{k}) = \begin{pmatrix} \mathcal{H}_{n,\pm i}(\mathbf{k}) & -i\Delta_0 s_y \\ i\Delta_0 s_y & -\mathcal{H}_{n,\pm i}^*(-\mathbf{k}) \end{pmatrix}.$$

$\mathcal{H}_{+i}(\mathbf{k})$  and  $\mathcal{H}_{-i}(\mathbf{k})$  are connected by time-reversal symmetry, leading to the absence of time-reversal symmetry within each block individually. To reveal the effective pairing of the superconductor, it is necessary to transform the Hamiltonian into the band basis. The normal state counterpart of block Hamiltonian  $H_{n,+i} = \int d^2\mathbf{k}[\Psi^\dagger(\mathbf{k})\mathcal{H}_{n,+i}(\mathbf{k})\Psi(\mathbf{k})]$  can be diagonalized by using the following expression

$$\Psi(\mathbf{k}) = \Phi_+(\mathbf{k})\Psi_+(\mathbf{k}) + \Phi_-(\mathbf{k})\Psi_-(\mathbf{k}), \quad (8)$$

where  $\Psi_+$  ( $\Psi_-$ ) represents the annihilation operator for the upper (lower) energy band, and  $\Phi_+$  ( $\Phi_-$ ) denotes the corresponding normalized wavefunction

$$\begin{aligned} \Phi_+(\mathbf{k}) &= \sqrt{\frac{1}{2\lambda_k(\lambda_k + \epsilon)}} \begin{pmatrix} \lambda_k + \epsilon \\ g_x + ig_y \end{pmatrix}, \\ \Phi_-(\mathbf{k}) &= \sqrt{\frac{1}{2\lambda_k(\lambda_k + \epsilon)}} \begin{pmatrix} -g_x + ig_y \\ \lambda_k + \epsilon \end{pmatrix}, \end{aligned} \quad (9)$$

where  $g_{x,y}$  are the  $x$  and  $y$  components of  $\mathbf{g}(\mathbf{k})$ , respectively. Therefore, the block BdG Hamiltonian  $H_{+i}(\mathbf{k})$  in the band basis reads

$$\begin{aligned} H_{+i}(\mathbf{k}) &= \xi_+(\mathbf{k})\Psi_+^\dagger(\mathbf{k})\Psi_+(\mathbf{k}) + \xi_-(\mathbf{k})\Psi_-^\dagger(\mathbf{k})\Psi_-(\mathbf{k}) \\ &+ \Delta_{++}(\mathbf{k})\Psi_+^\dagger(\mathbf{k})\Psi_+^\dagger(-\mathbf{k}) + \Delta_{+-}(\mathbf{k})\Psi_+^\dagger(\mathbf{k})\Psi_-^\dagger(-\mathbf{k}) \\ &+ \Delta_{--}(\mathbf{k})\Psi_-^\dagger(\mathbf{k})\Psi_-^\dagger(-\mathbf{k}) + \text{H.C.}, \end{aligned} \quad (10)$$

with

$$\begin{aligned} \xi_\pm(\mathbf{k}) &= -\epsilon_0(\mathbf{k}) \pm \lambda_k, \\ \Delta_{++}(\mathbf{k}) &= -\Delta_0 \frac{\alpha_{\text{CR}}}{\lambda_k} \left( -ik_x + ky \right)^3, \\ \Delta_{+-}(\mathbf{k}) &= -\Delta_0 \frac{\epsilon}{\lambda_k}, \\ \Delta_{--}(\mathbf{k}) &= -\Delta_0 \frac{\alpha_{\text{CR}}}{\lambda_k} \left( ik_x + ky \right)^3. \end{aligned}$$

Equation (10) reveals that the pairing  $\Delta_3$  not only induces the inter-band  $s$ -wave pairing but also the intra-band  $f_x \pm if_y$  pairing with opposite chirality for the upper and lower bands. Figure 2(b) shows that when the chemical potential  $\mu_B$  is within the hybridization gap, the Fermi surface is solely provided by the lower band. Therefore,  $H_{+i}(\mathbf{k})$  describes a  $f + if$  wave superconductor, while  $H_{-i}(\mathbf{k})$  corresponds to the  $f - if$  wave superconductor. These two sectors form a time-reversal invariant TSC with helical  $f$ -wave pairing.

Given that each subsector belongs to class D, we can determine a Chern number for both  $H_{+i}(\mathbf{k})$  and  $H_{-i}(\mathbf{k})$ , then define the mirror Chern number as  $n_M = (n_{+i} - n_{-i})/2$  [37–44], where  $n_{+i}$  and  $n_{-i}$  represent the Chern numbers of occupied bands of  $H_{+i}(\mathbf{k})$  and  $H_{-i}(\mathbf{k})$ , respectively. The topological condition is given by  $\varepsilon^2 > \mu^2 + \Delta_0^2$ . If the chemical potential lies within the hybridization gap, the mirror Chern number takes the value  $n_M = 3$  when the above topological condition is met.

To examine the Majorana edge modes, the continuous model is transformed into a tight-binding model on a square lattice. Figure 3(a) illustrates the spectral function for a semi-infinite geometry with  $\Delta_3$  pairing, revealing three pairs of helical Majorana edge modes when  $n_M = 3$ , a stark contrast to the linear Rashba SOC scenario [20].

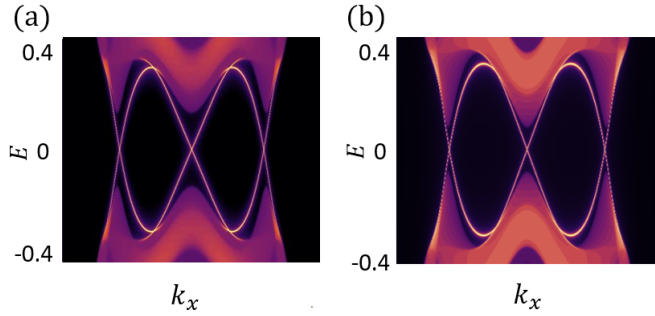


FIG. 3. Spectral function of a semi-infinite geometry with  $\Delta_3$  pairing when the chemical potential within the hybridization gap. (a) Only cubic Rashba SOC with  $\alpha_{CR} = 0.1$ . (b) Coexistence of linear Rashba and cubic Rashba SOC with  $\alpha_{CR} = 0.1, \alpha_{LR} = 0.1$ . Common parameters,  $\beta_0 = 0.5, \beta_1 = -1, \mu = 1.5, \varepsilon = 0.9, \Delta_0 = 0.5$ .

In general, cubic and linear Rashba SOC often occur together. It's crucial to understand how linear Rashba SOC influences the topological helical  $f$ -wave superconductivity brought on by the cubic Rashba SOC. Including linear Rashba SOC changes the landscape of superconducting pairings (detailed in the Supplemental Materials). In the case of  $\mu_A$ , boosting linear Rashba SOC first shrinks and then expands the  $\Delta_3$  region, while, in the case of  $\mu_B$  the  $\Delta_3$  region remains unchanged. As illustrated in Fig. 3(b), the inclusion of linear Rashba SOC does not alter the spectral function significantly; three pairs of gapless Majorana edge modes remain, indicating the stability of helical  $f$ -wave superconductivity.

**Nematic superconductivity.**—Pairing within the 2D representation (e.g., the  $E_u$  pairing in Table I) can lead to a nematic superconductor [45] characterized by broken rotational

symmetry in the gap amplitude. Such a phase can be experimentally verified, for instance, recent studies have identified odd-parity nematic superconductivity in doped  $\text{Bi}_2\text{Se}_3$  [46–51]. Our calculations indicate that the  $\Delta_4$  pairing can induce nematic superconductivity in this cubic Rashba spin-orbit coupled system. Figure 4(a) illustrates the anisotropic quasiparticle gap of  $\Delta_{4x}$  and  $\Delta_{4y}$  in the presence of only cubic Rashba SOC.  $\Delta_4$  pairing spontaneously reduces the point group symmetry from  $D_{4h}$  to  $C_{2h}$ . The quasiparticle gap displays six nodes, resulting in a nodal topological superconductor that supports flatband Majorana edge modes (See Supplemental Materials). For comparison, we also plot the quasiparticle gap in Fig. 4(b) when only linear Rashba SOC is present. In this scenario,  $\Delta_{4x}$  and  $\Delta_{4y}$  have two nodes along the  $k_y$  and  $k_x$  axes, respectively. Figures 4(c) and 4(d) demonstrate the quasiparticle gap with both linear and cubic Rashba SOC present. As the strength of the linear Rashba SOC increases relative to a fixed cubic Rashba SOC, the six nodes in the quasiparticle gap reduce to two nodes.

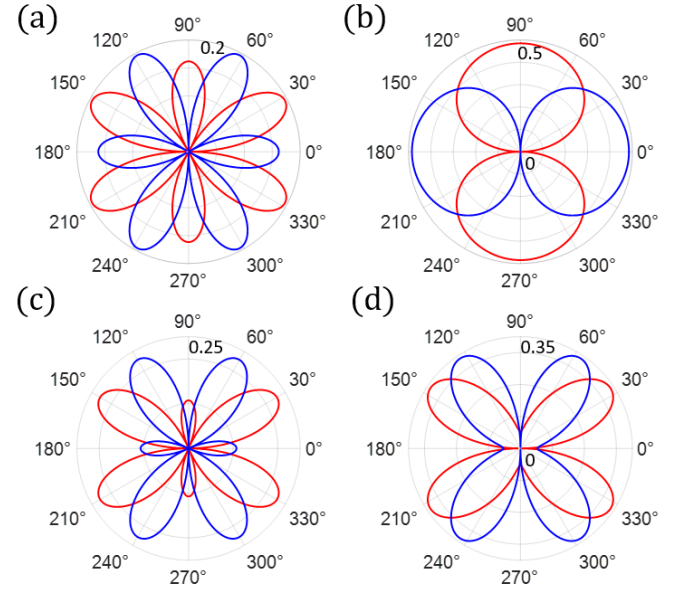


FIG. 4. Quasiparticle gap for  $\Delta_{4x}$  (marked by solid blue lines) and  $\Delta_{4y}$  (marked by solid red lines) pairings in the presence of linear and cubic Rashba SOC. Quasiparticle gap with cubic Rashba SOC of  $\alpha_{CR} = 0.1$  (a) and linear Rashba SOC  $\alpha_{LR} = 0.5$  (b), respectively. (c), (d) Quasiparticle gap with both linear and cubic Rashba SOC, where  $\alpha_{CR}$  is fixed at 0.1, and  $\alpha_{LR}$  takes values of 0.05, and 0.2, respectively. Common parameters,  $\beta_0 = 0, \beta_1 = -1, \mu = 2, \varepsilon = 0.9, \Delta_0 = 0.5$ .

**Discussions and conclusions.**—In this study, we present a new way to achieve helical  $f$ -wave superconductivity through odd-parity Cooper pairing in cubic Rashba superconductors that have broken local inversion symmetry. This type of superconductor has three pairs of gapless Majorana edge modes, protected by a mirror Chern number  $n_M = 3$ . Our calculations on an interacting bilayer Rashba model gives rise to a superconducting phase diagram with odd-parity pairings. Ad-



ditionally, we found that the topological helical  $f$ -wave superconductivity remains stable even with both linear and cubic Rashba terms. We also discuss the possibility of topological nematic superconductivity.

Our findings could potentially be seen at the interface between LaAlO<sub>3</sub> and SrTiO<sub>3</sub> oxides, where both linear and cubic Rashba SOC's can be controllable [26, 52], and superconductivity has been observed [53].

**Acknowledgments.**—We thank Zhongbo Yan, and Noah F. Q. Yuan for helpful discussions. This work was supported by the National Natural Science Foundation of China (NSFC, Grants No. 12074108, No. 12222402, and 12347101), the Chongqing Natural Science Foundation (Grants No. CSTB2023NSCQ-JQX0024 and No. CSTB2022NSCQ-MSX0568).

---

\* These authors contributed equally to this work.

† hu.lunhui.zju@gmail.com

‡ rcwang@cqu.edu.cn

§ donghuixu@cqu.edu.cn

- [1] Y. A. Bychkov and É. I. Rashba, Properties of a 2d electron gas with lifted spectral degeneracy, *JETP lett* **39**, 78 (1984).
- [2] A. Manchon, H. C. Koo, J. Nitta, S. M. Frolov, and R. A. Duine, New perspectives for Rashba spin-orbit coupling, *Nature Mater.* **14**, 871 (2015).
- [3] G. Bihlmayer, P. Noël, D. V. Vyalikh, E. V. Chulkov, and A. Manchon, Rashba-like physics in condensed matter, *Nat. Rev. Phys.* **4**, 642 (2022).
- [4] J. Sinova, D. Culcer, Q. Niu, N. A. Sinitsyn, T. Jungwirth, and A. H. MacDonald, Universal intrinsic spin Hall effect, *Phys. Rev. Lett.* **92**, 126603 (2004).
- [5] M. Z. Hasan and C. L. Kane, Colloquium: Topological insulators, *Rev. Mod. Phys.* **82**, 3045 (2010).
- [6] X.-L. Qi and S.-C. Zhang, Topological insulators and superconductors, *Rev. Mod. Phys.* **83**, 1057 (2011).
- [7] L. P. Gor'kov and E. I. Rashba, Superconducting 2D system with lifted spin degeneracy: Mixed singlet-triplet state, *Phys. Rev. Lett.* **87**, 037004 (2001).
- [8] S. K. Yip, Two-dimensional superconductivity with strong spin-orbit interaction, *Phys. Rev. B* **65**, 144508 (2002).
- [9] P. A. Frigeri, D. F. Agterberg, A. Koga, and M. Sigrist, Superconductivity without inversion symmetry: MnSi versus CePt<sub>3</sub>Si, *Phys. Rev. Lett.* **92**, 097001 (2004).
- [10] X. Zhang, Q. Liu, J.-W. Luo, A. J. Freeman, and A. Zunger, Hidden spin polarization in inversion-symmetric bulk crystals, *Nat. Phys.* **10**, 387 (2014).
- [11] K. Gottlieb, C.-Y. Lin, M. Serbyn, W. Zhang, C. L. Smallwood, C. Jozwiak, H. Eisaki, Z. Hussain, A. Vishwanath, and A. Lanzara, Revealing hidden spin-momentum locking in a high-temperature cuprate superconductor, *Science* **362**, 1271 (2018).
- [12] S. Khim, J. Landaeta, J. Banda, N. Bannor, M. Brando, P. Brydon, D. Hafner, R. Küchler, R. Cardoso-Gil, U. Stockert, et al., Field-induced transition within the superconducting state of CeRh<sub>2</sub>As<sub>2</sub>, *Science* **373**, 1012 (2021).
- [13] M. H. Fischer, M. Sigrist, D. F. Agterberg, and Y. Yanase, Superconductivity and local inversion-symmetry breaking, *Annual Review of Condensed Matter Physics* **14**, 153 (2023).
- [14] L. Fu and C. L. Kane, Superconducting proximity effect and majorana fermions at the surface of a topological insulator, *Phys. Rev. Lett.* **100**, 096407 (2008).
- [15] S. Fujimoto, Topological order and non-abelian statistics in noncentrosymmetric  $s$ -wave superconductors, *Phys. Rev. B* **77**, 220501 (2008).
- [16] M. Sato, Y. Takahashi, and S. Fujimoto, Non-Abelian topological order in  $s$ -wave superfluids of ultracold Fermionic atoms, *Phys. Rev. Lett.* **103**, 020401 (2009).
- [17] J. D. Sau, R. M. Lutchyn, S. Tewari, and S. Das Sarma, Generic new platform for topological quantum computation using semiconductor heterostructures, *Phys. Rev. Lett.* **104**, 040502 (2010).
- [18] J. Alicea, Majorana fermions in a tunable semiconductor device, *Phys. Rev. B* **81**, 125318 (2010).
- [19] C.-X. Liu and B. Trauzettel, Helical Dirac-Majorana interferometer in a superconductor/topological insulator sandwich structure, *Phys. Rev. B* **83**, 220510 (2011).
- [20] S. Nakosai, Y. Tanaka, and N. Nagaosa, Topological superconductivity in bilayer Rashba system, *Phys. Rev. Lett.* **108**, 147003 (2012).
- [21] F. Zhang, C. L. Kane, and E. J. Mele, Time-reversal-invariant topological superconductivity and Majorana Kramers pairs, *Phys. Rev. Lett.* **111**, 056402 (2013).
- [22] H. Nakamura, T. Koga, and T. Kimura, Experimental evidence of cubic Rashba effect in an inversion-symmetric oxide, *Phys. Rev. Lett.* **108**, 206601 (2012).
- [23] R. Moriya, K. Sawano, Y. Hoshi, S. Masubuchi, Y. Shiraki, A. Wild, C. Neumann, G. Abstreiter, D. Bougeard, T. Koga, and T. Machida, Cubic Rashba spin-orbit interaction of a two-dimensional hole gas in a strained-Ge/SiGe quantum well, *Phys. Rev. Lett.* **113**, 086601 (2014).
- [24] Y. Kim, R. M. Lutchyn, and C. Nayak, Origin and transport signatures of spin-orbit interactions in one- and two-dimensional SrTiO<sub>3</sub>-based heterostructures, *Phys. Rev. B* **87**, 245121 (2013).
- [25] P. Kim, K. T. Kang, G. Go, and J. H. Han, Nature of orbital and spin Rashba coupling in the surface bands of SrTiO<sub>3</sub> and KTaO<sub>3</sub>, *Phys. Rev. B* **90**, 205423 (2014).
- [26] W. Lin, L. Li, F. Doğan, C. Li, H. Rotella, X. Yu, B. Zhang, Y. Li, W. S. Lew, S. Wang, et al., Interface-based tuning of Rashba spin-orbit interaction in asymmetric oxide heterostructures with 3 d electrons, *Nat. Commun.* **10**, 3052 (2019).
- [27] D. Y. Usachov, I. A. Nechaev, G. Poelchen, M. Güttler, E. E. Krasovskii, S. Schulz, A. Generalov, K. Kliemt, A. Kraiker, C. Krellner, K. Kummer, S. Danzenbächer, C. Laubschat, A. P. Weber, J. Sánchez-Barriga, E. V. Chulkov, A. F. Santander-Syro, T. Imai, K. Miyamoto, T. Okuda, and D. V. Vyalikh, Cubic Rashba effect in the surface spin structure of rare-earth ternary materials, *Phys. Rev. Lett.* **124**, 237202 (2020).
- [28] H. J. Zhao, H. Nakamura, R. Arras, C. Paillard, P. Chen, J. Gosteau, X. Li, Y. Yang, and L. Bellaiche, Purely cubic spin splittings with persistent spin textures, *Phys. Rev. Lett.* **125**, 216405 (2020).
- [29] J. Schliemann and D. Loss, Spin-hall transport of heavy holes in III-V semiconductor quantum wells, *Phys. Rev. B* **71**, 085308 (2005).
- [30] O. Bleibaum and S. Wachsmuth, Spin hall effect in semiconductor heterostructures with cubic rashba spin-orbit interaction, *Phys. Rev. B* **74**, 195330 (2006).
- [31] X.-T. Peng, F. Lin, L. Chen, L. Li, D.-H. Xu, and J.-H. Sun, Tunable correlation effects of magnetic impurities by cubic Rashba spin-orbit coupling, *Phys. Rev. B* **107**, 165148 (2023).
- [32] L. Mao, J. Shi, Q. Niu, and C. Zhang, Superconducting phase with a chiral  $f$ -wave pairing symmetry and Majorana Fermions

- induced in a hole-doped semiconductor, *Phys. Rev. Lett.* **106**, 157003 (2011).
- [33] M. Alidoust, C. Shen, and I. Žutić, Cubic spin-orbit coupling and anomalous Josephson effect in planar junctions, *Phys. Rev. B* **103**, L060503 (2021).
- [34] M. Luethi, K. Laubscher, S. Bosco, D. Loss, and J. Klinovaja, Planar Josephson junctions in germanium: Effect of cubic spin-orbit interaction, *Phys. Rev. B* **107**, 035435 (2023).
- [35] L. Fu and E. Berg, Odd-parity topological superconductors: Theory and application to  $\text{Cu}_x\text{Bi}_2\text{Se}_3$ , *Phys. Rev. Lett.* **105**, 097001 (2010).
- [36] T. Hashimoto, S. Kobayashi, Y. Tanaka, and M. Sato, Superconductivity in doped Dirac semimetals, *Phys. Rev. B* **94**, 014510 (2016).
- [37] J. C. Y. Teo, L. Fu, and C. L. Kane, Surface states and topological invariants in three-dimensional topological insulators: Application to  $\text{Bi}_{1-x}\text{Sb}_x$ , *Phys. Rev. B* **78**, 045426 (2008).
- [38] F. Zhang, C. L. Kane, and E. J. Mele, Topological mirror superconductivity, *Phys. Rev. Lett.* **111**, 056403 (2013).
- [39] Y. Ueno, A. Yamakage, Y. Tanaka, and M. Sato, Symmetry-protected Majorana Fermions in topological crystalline superconductors: Theory and application to  $\text{Sr}_2\text{RuO}_4$ , *Phys. Rev. Lett.* **111**, 087002 (2013).
- [40] C.-K. Chiu, H. Yao, and S. Ryu, Classification of topological insulators and superconductors in the presence of reflection symmetry, *Phys. Rev. B* **88**, 075142 (2013).
- [41] Y. Tsutsumi, M. Ishikawa, T. Kawakami, T. Mizushima, M. Sato, M. Ichioka, and K. Machida,  $\text{UPt}_3$  as a topological crystalline superconductor, *journal of the physical society of japan* **82**, 113707 (2013).
- [42] K. Shiozaki and M. Sato, Topology of crystalline insulators and superconductors, *Phys. Rev. B* **90**, 165114 (2014).
- [43] Y. Ando and L. Fu, Topological crystalline insulators and topological superconductors: From concepts to materials, *Annu. Rev. Condens. Matter Phys.* **6**, 361 (2015).
- [44] T. Yoshida, M. Sgrist, and Y. Yanase, Topological crystalline superconductivity in locally noncentrosymmetric multilayer superconductors, *Phys. Rev. Lett.* **115**, 027001 (2015).
- [45] L. Fu, Odd-parity topological superconductor with nematic order: Application to  $\text{Cu}_x\text{Bi}_2\text{Se}_3$ , *Phys. Rev. B* **90**, 100509 (2014).
- [46] K. Matano, M. Kriener, K. Segawa, Y. Ando, and G.-q. Zheng, Spin-rotation symmetry breaking in the superconducting state of  $\text{Cu}_x\text{Bi}_2\text{Se}_3$ , *Nature Physics* **12**, 852 (2016).
- [47] S. Yonezawa, K. Tajiri, S. Nakata, Y. Nagai, Z. Wang, K. Segawa, Y. Ando, and Y. Maeno, Thermodynamic evidence for nematic superconductivity in  $\text{Cu}_x\text{Bi}_2\text{Se}_3$ , *Nature Physics* **13**, 123 (2017).
- [48] T. Asaba, B. J. Lawson, C. Tinsman, L. Chen, P. Corbae, G. Li, Y. Qiu, Y. S. Hor, L. Fu, and L. Li, Rotational symmetry breaking in a trigonal superconductor Nb-doped  $\text{Bi}_2\text{Se}_3$ , *Phys. Rev. X* **7**, 011009 (2017).
- [49] Y. Pan, A. Nikitin, G. Araizi, Y. Huang, Y. Matsushita, T. Naka, and A. De Visser, Rotational symmetry breaking in the topological superconductor  $\text{Sr}_x\text{Bi}_2\text{Se}_3$  probed by upper-critical field experiments, *Scientific reports* **6**, 1 (2016).
- [50] G. Du, Y. Li, J. Schneeloch, R. Zhong, G. Gu, H. Yang, H. Lin, and H.-H. Wen, Superconductivity with two-fold symmetry in topological superconductor  $\text{Sr}_x\text{Bi}_2\text{Se}_3$ , *Science China Physics, Mechanics & Astronomy* **60**, 1 (2017).
- [51] R. Tao, Y.-J. Yan, X. Liu, Z.-W. Wang, Y. Ando, Q.-H. Wang, T. Zhang, and D.-L. Feng, Direct visualization of the nematic superconductivity in  $\text{Cu}_x\text{Bi}_2\text{Se}_3$ , *Phys. Rev. X* **8**, 041024 (2018).
- [52] A. D. Caviglia, M. Gabay, S. Gariglio, N. Reyren, C. Cancellieri, and J.-M. Triscone, Tunable Rashba spin-orbit interaction at oxide interfaces, *Phys. Rev. Lett.* **104**, 126803 (2010).
- [53] N. Reyren, S. Thiel, A. Caviglia, L. F. Kourkoutis, G. Hammerl, C. Richter, C. W. Schneider, T. Kopp, A.-S. Ruetschi, D. Jaccard, et al., Superconducting interfaces between insulating oxides, *Science* **317**, 1196 (2007).